



2nd Advanced Optical Metrology Compendium

Advanced Optical Metrology

Geoscience | Corrosion | Particles | Additive Manufacturing: Metallurgy, Cut Analysis & Porosity



EVIDENT
OLYMPUS

WILEY

The latest eBook from **Advanced Optical Metrology**.
Download for free.

This compendium includes a collection of optical metrology papers, a repository of teaching materials, and instructions on how to publish scientific achievements.

With the aim of improving communication between fundamental research and industrial applications in the field of optical metrology we have collected and organized existing information and made it more accessible and useful for researchers and practitioners.

EVIDENT
OLYMPUS

WILEY

An Evaluation of the Mechanical Properties, Microstructures, and Strengthening Mechanisms of Pure Mg Processed by High-Pressure Torsion at Different Temperatures

Zhuoliang Li, Hua Ding,* Yi Huang,* and Terence G. Langdon

Pure Mg samples are processed by high-pressure torsion (HPT) for up to ten turns at temperatures of 293 and 423 K. The microstructures of these samples are significantly refined and bimodal structures are obtained after 10 turns of HPT processing at both 293 and 423 K. Tensile experiments are conducted at room temperature to reveal the mechanical properties of pure Mg subjected to HPT processing at different temperatures. The yield strength increases with increasing numbers of turns after processing at 293 K whereas the yield strength shows almost no variation with increasing numbers of turns at 423 K. Pure Mg processed at 423 K exhibits a higher strain hardening ability and a larger uniform elongation than after processing at 293 K. Calculations show that the grain size, bimodal structure, and dislocation density are the main factors affecting both the yield strength of the material and the work hardening behavior.

operations, and relative ease in recycling.^[1] Accordingly, Mg and Mg alloys have many opportunities for use in the fields of automobiles, electronic communications, as biodegradable implants in medicine and in many aerospace applications. Nevertheless, Mg and Mg alloys have an overall problem of low strength and this seriously hinders their use.^[2] According to the Hall–Petch^[3,4] relationship, grain refinement is an efficient method for enhancing the yield strength of Mg and Mg alloys because hexagonal close-packed (HCP) metals such as Mg exhibit a larger value of the Hall–Petch coefficient compared to body-centered cubic (BCC) and face-centered cubic (FCC) metals.^[5–8]

The most efficient procedure for reducing the grain sizes of metallic materials is through the application of severe plastic deformation (SPD) techniques which may be used in producing bulk materials with ultrafine-grained microstructures.^[9–14] Equal-channel angular pressing (ECAP)^[15] and high-pressure torsion (HPT)^[16] are among the most popular SPD techniques for achieving significant grain refinement. However, Mg alloys often exhibit major cracking during ECAP processing at room temperature due to limited availability of slip systems and this means the processing

1. Introduction

As the lightest metallic structural material, with a density of 2/3 of aluminum and 1/4 of steel, magnesium and its alloys attract significant attention from materials researchers. Magnesium and Mg alloys have the advantages of high specific strength and specific stiffness, good electrical and thermal conductivity, excellent damping capacity and electromagnetic shielding capability, good biocompatibility, a potential for use in superplastic forming

Z. Li, H. Ding
School of Material Science and Engineering
Northeastern University
Shenyang 110819, China
E-mail: dingh@smm.neu.edu.cn

Z. Li, H. Ding
Key Laboratory of Lightweight Structural Materials, Liaoning Province
Northeastern University
Shenyang 110819, China

 The ORCID identification number(s) for the author(s) of this article can be found under <https://doi.org/10.1002/adem.202200799>.

© 2022 The Authors. Advanced Engineering Materials published by Wiley-VCH GmbH. This is an open access article under the terms of the Creative Commons Attribution-NonCommercial-NoDerivs License, which permits use and distribution in any medium, provided the original work is properly cited, the use is non-commercial and no modifications or adaptations are made.

DOI: 10.1002/adem.202200799

Z. Li
HuiBo Heat Energy Engineering Technology Center
Shenyang Academy of Instrumentation Science Co., Ltd
Shenyang 110043, China

Y. Huang
Department of Design and Engineering
Faculty of Science and Technology
Bournemouth University
Poole, Dorset BH12 5BB, UK
E-mail: yhuang2@bournemouth.ac.uk

Y. Huang, T. G. Langdon
Materials Research Group
Department of Mechanical Engineering
University of Southampton
Southampton SO17 1BJ, UK

temperature is an important factor in controlling the grain refinement and improving the strength.^[17,18] Through the use of concurrent torsional shear deformation and the imposition of a high hydrostatic stress, experiments show that the alternative procedure of HPT has a major advantage over ECAP in the processing of hard-to-deform materials such as Mg alloys at low temperatures.^[19,20] Furthermore, HPT is also the most efficient SPD method in achieving significant grain refinement due to the larger shear strains that may be readily applied. Several experiments have demonstrated that, by comparison with ECAP, HPT processing produces both smaller grain sizes^[21,22] and higher fractions of grain boundaries having high angles of misorientation.^[23]

Many reports are now available describing the microstructural features, the microhardness, and the texture evolution in Mg and Mg alloys when subjected to HPT processing.^[19,20,24–57] There is also a recent review describing the characteristics associated with the processing of magnesium and its alloys by HPT.^[58] A careful examination of these various reports reveals several interesting trends. In the room temperature processing of pure Mg, it was found that the microhardness increased significantly after 1/8 turn but thereafter there was no further increase in microhardness with increasing numbers of rotations.^[35] Tensile testing of HPT-processed pure Mg and fully recrystallized pure Mg showed the potential for achieving exceptionally high tensile ductilities.^[29,36] The Mg–Gd–Y–Zn–Zr alloy was successfully processed by HPT at room temperature for a range of turns from 1/8 to 16 and the results showed that grain refinement was the dominant factor for hardening with second-phase particles distributed homogeneously with increasing turns of HPT.^[45] In order to evaluate the effect of the deformation strain rate on the microstructure and hardness evolution, an AZ31 alloy was processed by HPT at 453 K using three different rotation rates and the results showed that the strain rate has only a minor effect on hardness and average grain size.^[30] For Mg alloys, there are reports on the effects of the numbers of HPT rotations on the microstructural development in AZ80 and AZ31 alloys at room temperature^[27,37] and it was found that the average grain sizes of the alloys were significantly decreased with increasing turns in HPT. The effect of processing temperatures on the microstructures and mechanical properties of AZ31 were investigated by HPT processing from 296 to 473 K^[19,32] with results showing that processing at 296 and 373 K leads to significant grain refinement whereas processing at 473 K is accompanied by grain growth during the processing operation. There is also a report on HPT processing of an Mg–9%Al alloy at room temperature and 423 K where superplasticity was achieved after processing

at 423 K with a maximum elongation of 810% at a tensile testing temperature of 473 K.^[26]

A general conclusion from a review of the available data is that most of the studies conducted to date on HPT processing of Mg and Mg alloys under different temperatures are focused exclusively on the evolution of hardness and grain refinement. By contrast, there is only very limited information on the influence of the HPT processing temperature on the strengthening mechanisms of Mg and Mg alloys and there is an almost total absence of quantitative research on the relevant strengthening mechanisms. Furthermore, although studies of the strain hardening behavior of materials are important for practical application, there remains a lack of data on the work hardening behavior of Mg and Mg alloys when processed by HPT at different temperatures. Accordingly, the present research was undertaken to process pure Mg at temperatures of 293 and 423 K, to examine the effect of the processing temperature on the mechanical behavior and microstructure, and also to investigate the temperature effect on the work hardening behavior and the contributions from different strengthening mechanisms to the measured yield strengths.

2. Experimental Section

The experiments were conducted on commercially pure Mg of 99.9% purity using the procedure illustrated schematically in **Figure 1a**. It is important to note that the microstructures produced in the HPT processing of magnesium are dependent upon the purity level of the material. Specifically, tests showed that commercial purity Mg, as used in the present investigation, produces a finer grain size than high purity Mg because the presence of the impurity elements plays a significant role in restricting the movement of dislocations and in enhancing the advent of dynamic recrystallization.^[56]

The pure Mg was initially forged at 673 K with a total reduction of 50%, and then rod specimens with diameters of 9.8 mm were cut from the forged sample along the forging direction using wire cutting. For HPT processing, disks were cut from these rods with thicknesses of ≈ 0.8 mm and these disks were then subjected to HPT processing under a pressure of 6.0 GPa with an anvil rotation speed at 1 rpm at temperatures of either 293 or 423 K. The HPT facility operated under quasiconstrained conditions where there is a small outflow of material around the periphery of the disk during the pressing operation.^[59,60]

Samples were processed by HPT to 1/8, 1, and 10 turns and then the top surfaces of the disks were mechanically polished.

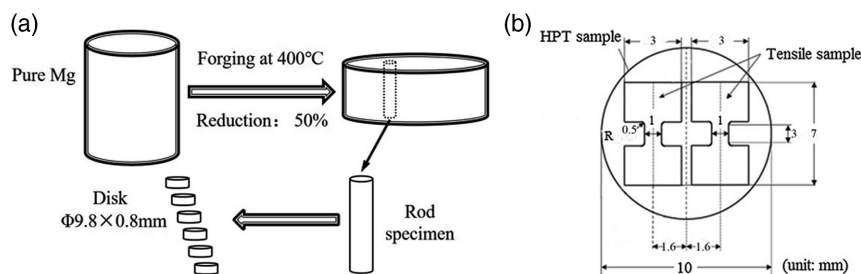


Figure 1. Schematic illustrations of a) the procedure for HPT sample preparation and b) the tensile testing samples cut from the HPT-processed disks.

The Vickers microhardness, Hv, was measured on the polished surface along randomly selected diameters using a load of 50 gf, a dwell time of 10 s, and with a distance between each indentation of 0.5 mm. Two tensile specimens were cut from each disk at off-center positions as illustrated in Figure 1b and these specimens were pulled in tension to failure at room temperature with an initial strain rate of $1.0 \times 10^{-3} \text{ s}^{-1}$. For microstructural observations, the HPT-processed disks were polished using abrasive papers of 2000#, 3000#, and 5000# and then polished with diamond paste at a size of 0.1 μm . An acetic–picric acid solution was used for etching of the polished surfaces and electron back-scatter diffraction (EBSD) results were obtained using an Ultra Plus field emission scanning electron microscope (SEM). The images were taken at the half radius of the HPT disks and these same positions were used for X-Ray measurements and observations by transmission electron microscopy (TEM). A TD-3500 X-Ray diffractometer and a Tecnai G220 microscope were used for the microstructural characterization.

3. Experimental Results

3.1. Microstructures Before and After HPT Processing

Figure 2a shows the initial microstructure of the pure Mg before HPT processing where there was a coarse grain structure with an average grain size of $\approx 45 \mu\text{m}$ and no obvious twin structure. During the high-temperature forging process there was dynamic recrystallization within the material so that the fraction of high-angle grain boundaries (HAGBs) was very high at $\approx 93.1\%$ as

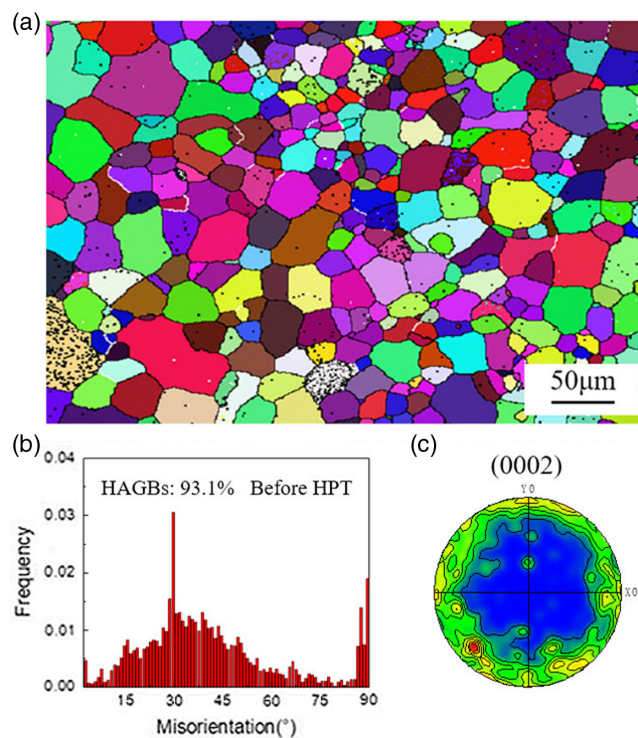


Figure 2. Microstructure of pure Mg before HPT: a) IPF figure; b) misorientation distribution; c) pole figure.

shown in Figure 2b. In addition, there was a dominant cylindrical texture as shown by the pole figure in Figure 2c.

The EBSD figures in Figure 3 provide a clear illustration of the microstructural evolution of the samples after HPT processing to different numbers of rotations at the two different processing temperatures. It is important to note that significant grain refinements were achieved in the ten turns sample for both processing temperatures. Specifically, as shown in Figure 3a,c,e, for HPT processing at 293 K there was no significant grain refinement after 1/8 turn with an average grain size of $\approx 32.9 \mu\text{m}$ but the grains were refined to $\approx 9.3 \mu\text{m}$ after one turn and then after ten turns there was a bimodal state with fine grains ($\approx 2\text{--}3 \mu\text{m}$) mixed with coarser grains ($\approx 8\text{--}10 \mu\text{m}$). Earlier research showed that dynamic recrystallization may occur in pure Mg during HPT processing at room temperature^[25,29] and this is consistent with the present results. Close inspection of Figure 3b,d,f shows that significant recrystallization occurred in the samples processed by HPT at 423 K. After 1/8 and 1 turn, the grain refinement was more significant than in the samples processed at 293 K with finer grains and there is a tendency toward bimodal grain distributions. Further processing to ten turns established the bimodal grain distribution in Figure 3f and it appears that the coarser grains have experienced some grain growth. The volume fractions of the coarser grains and the fine grains in samples with bimodal grain distributions, and the corresponding average grain sizes of the fine and coarse grains, are summarized in Table 1 where the bimodal distributions include the ten turns sample processed at 293 K and all samples processed at 423 K.

For the two different processing temperatures used in these experiments, the characteristics of the microstructural refinement are different. For HPT processing at 293 K, the coarse grains are gradually refined with the accumulation of strain where, following the classic model for grain refinement in cold deformation,^[61] the strain leads to the movement of dislocations to form low-angle grain boundaries (LAGBs) and these LAGBs continuously absorb dislocations and transform into stable HAGBs. This is similar to the principles of grain refinement proposed for processing by ECAP.^[62] By contrast, for HPT processing at 423 K the grain refinement is achieved through dynamic recrystallization leading to a well-defined bimodal structure where fine gains change very little with increasing numbers of HPT turns. It is apparent from Table 1 that the volume fraction of coarse grains and fine grains in the 10 turns sample processed at 293 K is 55.6% and 44.4%, respectively, and this is very similar to the values of 45.9% and 54.1% for the ten turns sample processed at 423 K.

The relevant pole figures are shown in Figure 4 after processing at different temperatures where it is apparent that a basal texture is formed in pure Mg when processing by HPT at either 293 or 423 K. At 293 K the maximum intensities of the texture decrease through the sequence of 15.5, 14.9, and 10.5 when HPT is increased through 1/8, 1, and 10 turns, respectively, where the significant decrease at ten turns is due to the advent of dynamic recrystallization, as shown in Figure 4a,c,e. In processing at 423 K, Figure 4b,d,f shows that the intensity values are 11.2 and 10.8 after 1/8 and 1 turn and then the intensity remains essentially constant through ten turns where the initial values are lower than at 293 K because of the continuous dynamic

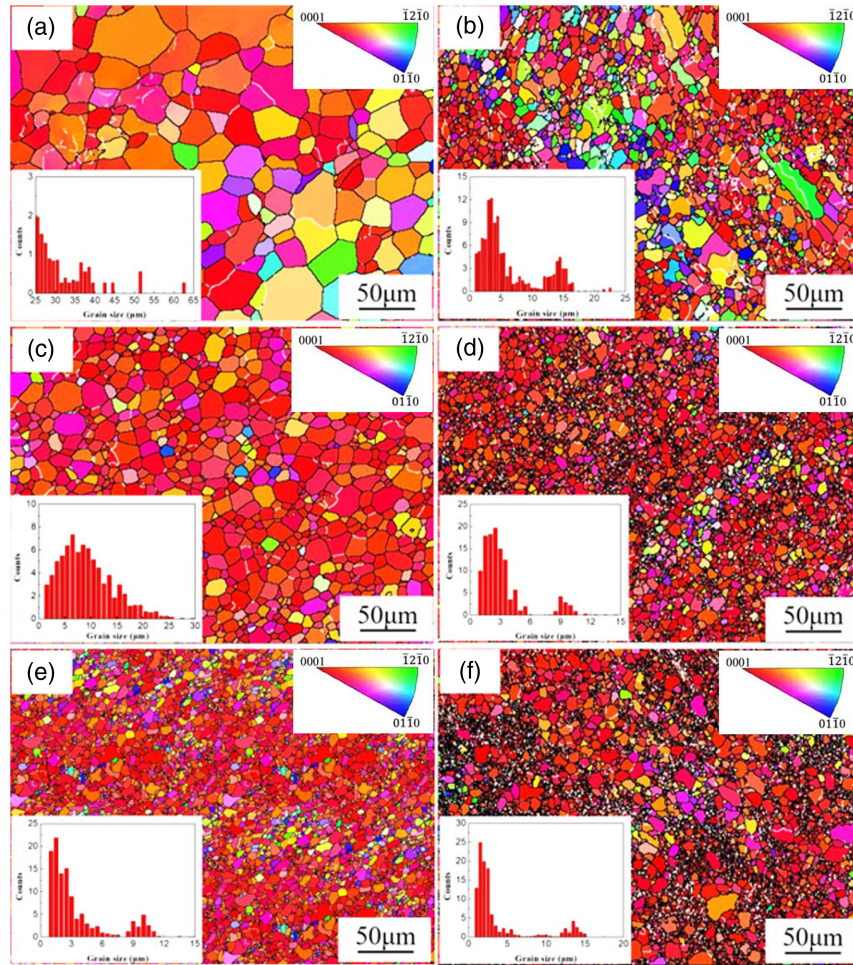


Figure 3. IPF pictures of the samples after HPT processing at different conditions: a) 1/8 turn at 293 K; b) 1/8 turn at 423 K; c) 1 turn at 293 K; d) 1 turn at 423 K; e) 10 turns at 293 K; f) 10 turns at 423 K.

Table 1. Average grain sizes of samples after HPT processing.

Grain size	Temperature [K]	Turns of HPT		
		1/8	1	10
Average grain size (μm)/volume fraction	293	32.9	9.3	2.5/44.4%
	423	3.9/38.9%	2.7/44.7%	2.2/45.9%
		15.9/61.1%	11.0/55.3%	13.6/54.1%

recrystallization. These textures are consistent with the expectations for processing by HPT as documented in a recent review.^[63]

3.2. Dislocation Densities After HPT Processing

The dislocation densities of the samples after HPT processing under different conditions were calculated using X-Ray diffraction (XRD).^[64] Figure 5a,c shows that the XRD results of the samples processed at 293 and 423 K where the analysis of the diffraction pattern assumes that the width of the peaks is affected

by the grain size so that the dislocation density is then obtained by calculating the microstrain within the material.^[65] The microstrain is obtained from the slopes of the $2\sin\theta/\lambda - \delta\cos\theta/\lambda$ curves as shown in Figure 5b,d and the dislocation density, ρ , is calculated from the expression

$$\rho \cong \frac{4\pi e^2}{Cb^2} \quad (1)$$

where e is the microstrain, b is the Burgers vector of pure Mg, and C is a coefficient which is taken as 0.19483.^[64]

The calculated values of the dislocation densities are shown in Table 2. For the samples processed at 293 K, the values of ρ increase gradually with increasing numbers of turns with all values lying above 10^{15} m^{-2} whereas for samples processed at 423 K the dislocation densities are in the range of $10^{14} - 10^{15} \text{ m}^{-2}$. Thus, the dislocation densities of the samples processed at 423 K are much lower than those processed at 293 K because, although the shear strain introduced by HPT processing at 423 K produces rapid dislocation multiplication, this is more than offset by the reduction in dislocation density due to the intense dynamic recrystallization.

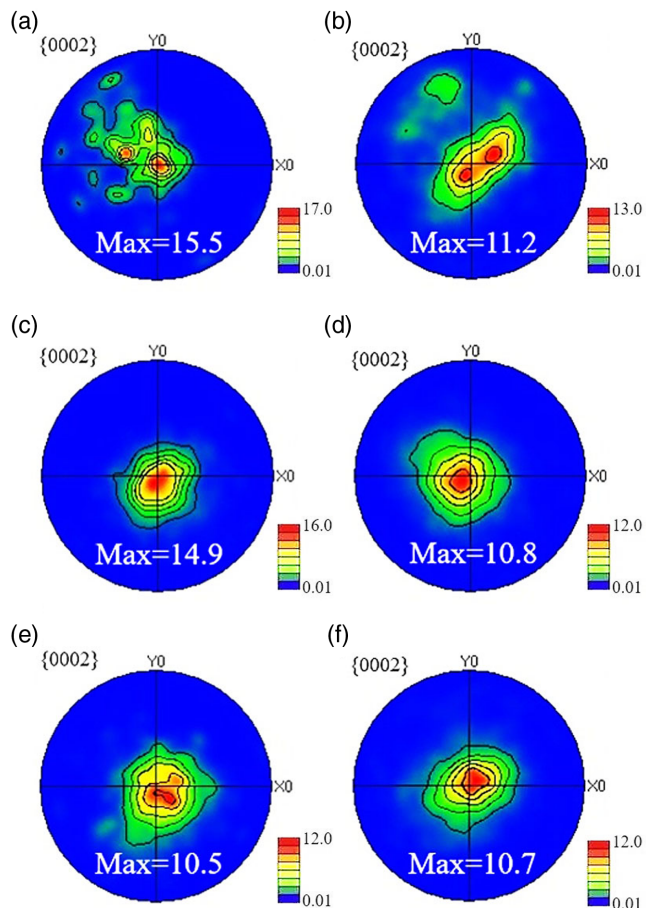


Figure 4. The {0001} pole figures of the samples after HPT processing for a) 1/8 turn at 293 K; b) 1/8 turn at 423 K; c) 1 turn at 293 K; d) 1 turn at 423 K; e) 10 turns at 293 K; f) 10 turns at 423 K.

3.3. Microhardness Values and Tensile Testing

Prior to HPT processing, the Vickers microhardness of the pure Mg was measured as ≈ 40 Hv. The Vickers microhardness results after HPT processing are shown in **Figure 6** for HPT temperatures of a) 293 and b) 423 K, respectively, where the abscissa corresponds to the distance from the disk center. It can be seen from **Figure 6a** that after 1/8 turn of HPT at 293 K the microhardness reached ≈ 52 Hv at the disk edge area but with additional HPT processing the microhardness values at the edge decreased to ≈ 47 Hv after ten turns. In the central region the hardness values are much lower after 1/8 and 1 turn due to the limited deformation in this region but after ten turns there is no evidence for a lower value in the central region. This latter result is consistent with the prediction from strain gradient plasticity modeling which demonstrates the gradual evolution to a homogeneous microstructure across disks subjected to HPT processing.^[66] In **Figure 6b**, the microhardness values are higher than in the unprocessed material after processing at 423 K but there is no clear dependence on the numbers of imposed rotations.

The room temperature engineering stress–strain curves are shown in **Figure 7** after HPT processing at a) 293 and

b) 423 K. The measured yield strength of the 1/8 turn sample was ≈ 112 MPa and this increased to ≈ 148 MPa after ten turns. Although the yield strength of the samples after HPT at 293 K increased with increasing numbers of turns, the ultimate tensile strength (UTS) of the 1/8 turn sample was much higher than for the one and ten turns sample. There is a different trend for samples processed at 423 K as shown in **Figure 7b** where there is no obvious difference in strength for the engineering stress–strain curves of samples processed through different numbers of turns. Thus, after HPT processing at 423 K all samples displayed a yield strength of ≈ 110 MPa regardless of the numbers of turns. With reference to the basal textures shown earlier in **Figure 4**, it is important to note that the basal texture places the grains in a hard-to-deform orientation which is beneficial in achieving a higher yield strength. Thus, the present results are consistent with earlier data showing texture strengthening in pure magnesium along the deformation direction of the material^[49] where the basal texture suppresses basal slip and promotes the onset of nonbasal slip systems.

In order to evaluate the onset of localized deformation during tensile testing, it is necessary to estimate the rate of work hardening.^[67] As shown in **Figure 8a** for materials processed by HPT at 293 K, the work hardening rate of the 1/8 turn sample decreased rapidly after a short work hardening process whereas the work hardening rates of the one and ten turns sample were quite low after true strains beyond ≈ 0.1 . For samples processed by HPT at 423 K in **Figure 8b**, all samples have higher work hardening rates at true strains beyond ≈ 0.1 . Therefore, a comparison of **Figure 7a,b** reveals a greater uniformity in elongation in the samples processed by HPT at 473 K by comparison with those processed by HPT at 293 K.

4. Discussion

4.1. Differences in the Uniform Elongation

The mechanical behavior of pure magnesium after HPT processing at different temperatures exhibited significant differences. As shown in **Figure 8**, the samples processed at 423 K displayed higher work hardening ability than the samples processed at 293 K. For the samples processed at 293 K, both the work hardening rate and the uniform elongation were low whereas the samples processed at 423 K exhibited longer uniform elongations.

The strain hardening processes of pure Mg are mainly controlled by dislocations. At 293 K there was a high density of dislocations after 1/8 turn with $\rho > 10^{15} \text{ m}^{-2}$ as shown in **Table 2**. This high density tends to limit the ability for dislocation multiplication during tensile testing at room temperature. Therefore, the work hardening rate of the 1/8 turn sample decreased rapidly after a short work hardening process, where this is similar to the conventional tensile deformation behavior of nanosized materials.^[68] With increasing HPT turns the dislocation densities of pure Mg were continuously enhanced with the result that the uniform elongations of the one and ten turns sample were very low.

Figure 9 shows TEM images of samples after processing at the two different temperatures and through different numbers of

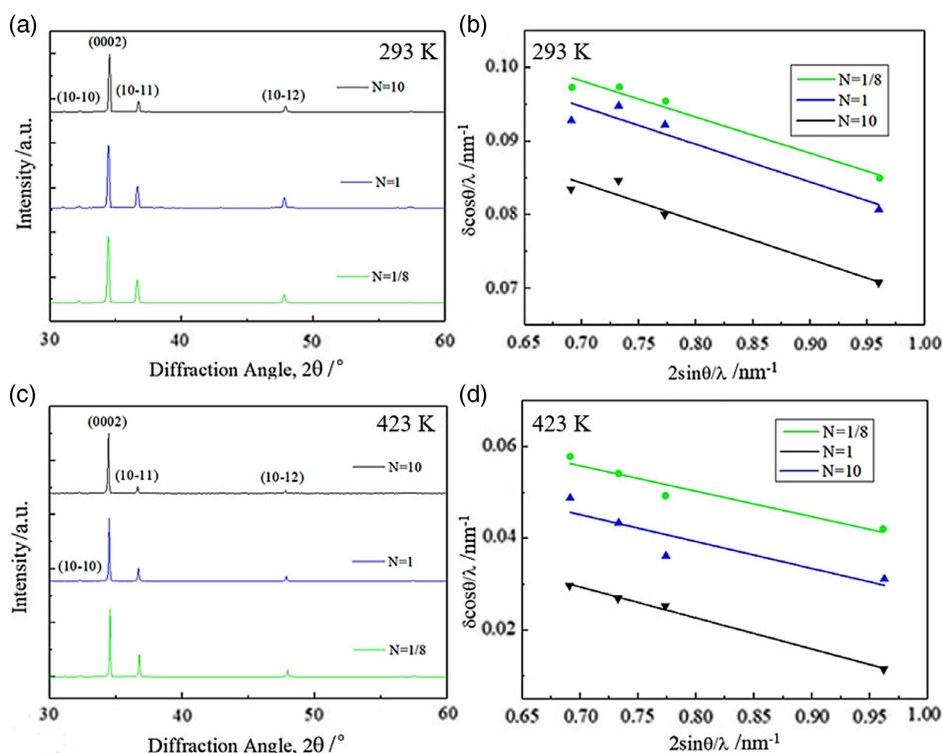


Figure 5. The XRD results of the samples after HPT and the $2\sin\theta/\lambda - \delta\cos\theta/\lambda$ curves for dislocation density calculations.

Table 2. Dislocation densities after HPT processing.

HPT parameters	Temperature [K]	Turns of HPT		
		1/8	1	10
Dislocation density [m^{-2}]	293	1.98×10^{15}	2.62×10^{15}	3.26×10^{15}
	423	7.07×10^{14}	3.21×10^{14}	2.96×10^{14}

turns. Figure 9b,d,f shows that after HPT processing at the elevated temperature of 423 K the dislocation density was relatively low due to dynamic recrystallization and dislocation multiplication occurred reasonably easily. In Figure 9a,c,e, dislocation

entanglements were obvious in samples processed at the low temperature of 293 K. This means that the 423 K samples should show an obvious work hardening ability during tensile deformation with higher uniform elongations.

In addition, studies confirmed that the development of a bimodal structure in Mg and Mg alloys is beneficial in restraining the formation and extension of cracks during deformation so that the uniform elongation is improved.^[69–71] Although there are reports of the development of bimodal structures in Mg and its alloys after HPT processing, it appears that there are no analyses documenting the influence of the bimodal structure on the mechanical properties and especially on the uniform

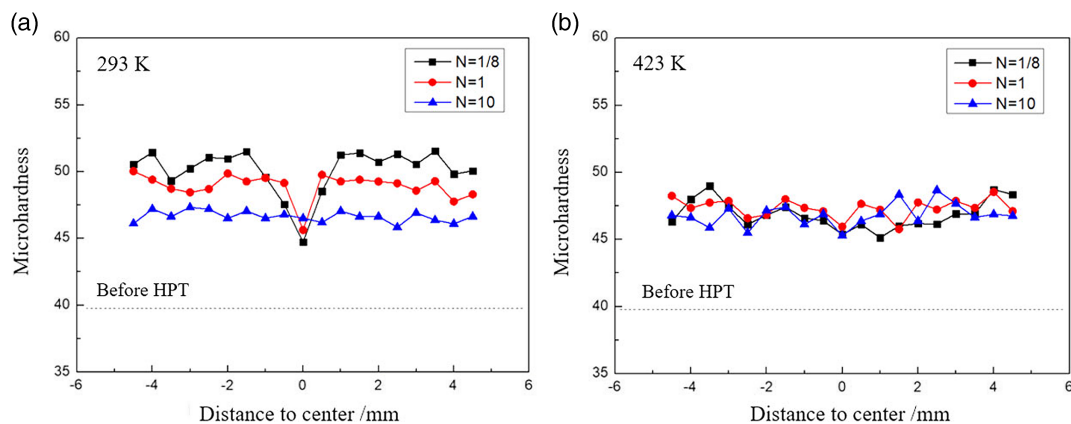


Figure 6. Vickers microhardness along selected diameters of Mg disks processed by HPT at temperatures of a) 293 and b) 423 K.

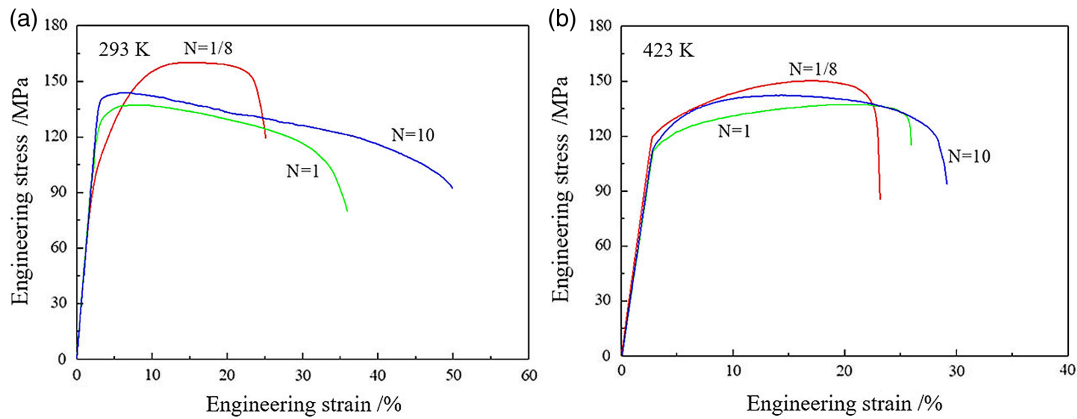


Figure 7. Engineering stress–strain curves of the samples processed by HPT for different numbers of turns at temperatures of a) 293 and b) 423 K.

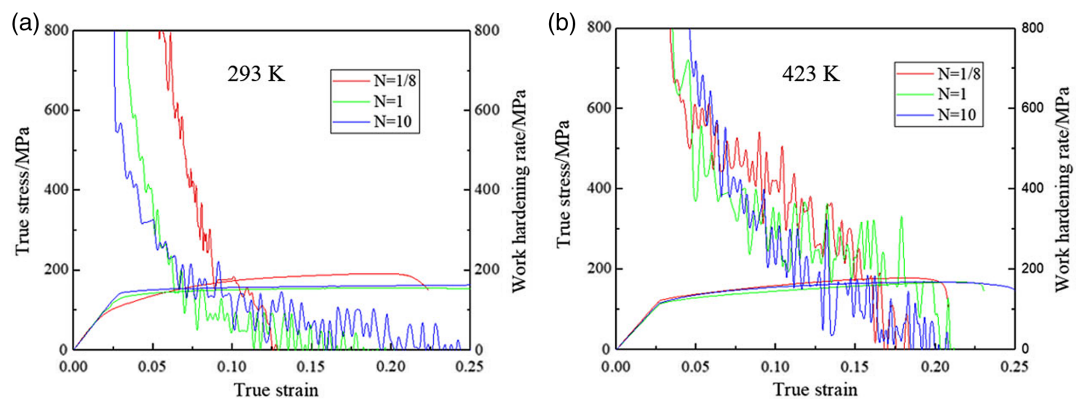


Figure 8. True strain–true stress and work hardening rate curves of samples processed by HPT at temperatures of a) 293 and b) 423 K.

elongation and work hardening behavior.^[31,47] In the present study, a bimodal structure was formed in pure Mg at 293 K when the numbers of HPT turns reached ten but the bimodal structure was present after processing at 423 K even after only 1/8 turn. These differences in the bimodal character of the microstructure, and the differences in the dislocation densities, are the main factors accounting for the different strain hardening behavior of pure Mg after HPT processing at different temperatures.

4.2. The Nature of the Strengthening Mechanisms

According to the engineering stress–engineering strain curves in Figure 7, the yield strengths of the samples processed at 293 K were higher than the samples processed at 423 K. With increasing numbers of HPT turns, the yield strengths of the 293 K samples increased whereas the yield strengths of the 423 K samples remained reasonably constant. The texture evolutions in samples processed by HPT at 293 and 473 K show the formation of the same basal texture in Figure 4, so that there is almost no different texture strengthening in samples processed by HPT at 293 and 473 K. The analysis now examines the main factors affecting the yield strength due to the different HPT processing temperatures of 293 and 473 K where these are grain boundary strengthening (σ_{gb}) and dislocation strengthening (σ_{dis}).

Through a conventional superposition of these contributions, the yield strength may be reasonably expressed by the relationship

$$\sigma_{0.2} = \sigma_0 + \sigma_{gb} + \sigma_{dis} \quad (2)$$

where σ_0 is the friction stress of pure Mg having a value of ≈ 31 MPa.^[72]

The contribution of grain size to the strength of a material can be expressed through the Hall–Petch relationship so that

$$\sigma_{gb} = kd^{-1/2} \quad (3)$$

where d is the average grain size of the material and, following calculations of the SPD processing for pure Mg, the value of the Hall–Petch constant k is taken as $0.17 \text{ MPa m}^{-1/2}$.^[73] Due to the bimodal structure formed in the pure Mg after HPT processing, the contributions of grain boundary strengthening to the yield strength were obtained by making separate calculations of the yield strengths of the fine and coarse grains, respectively. These strengths were multiplied by the corresponding volume fractions of the fine and coarse grains and the sum of the two results was then used as the overall contribution of grain boundary strengthening to the yield strength.

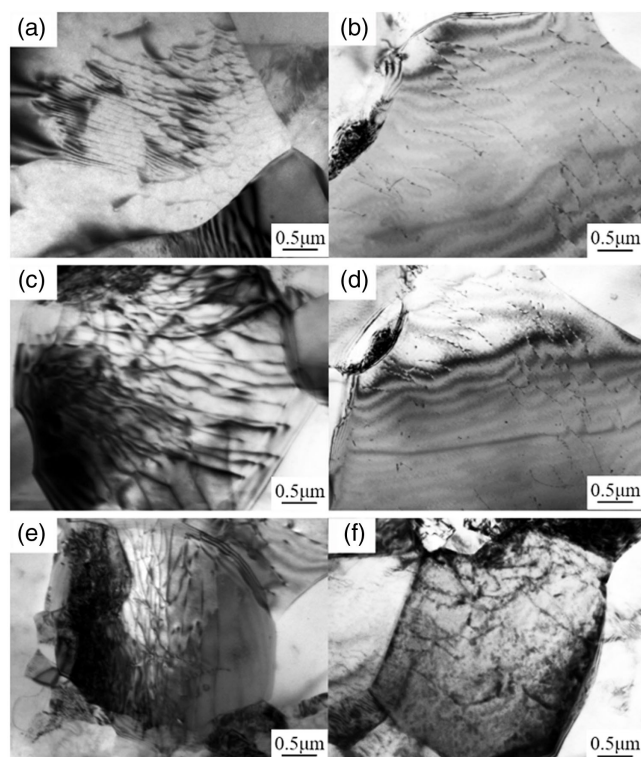


Figure 9. TEM images of samples after HPT processing through different turns and temperatures: a) 1/8 turn at 293 K, b) 1/8 turn at 423 K, c) 1 turn at 293 K, d) 1 turn at 423 K, e) 10 turns at 293 K, and f) 10 turns at 423 K.

The contribution of the dislocation density to the yield strength was expressed by the Taylor relationship so that^[74]

$$\sigma_{\text{dis}} = M\alpha Gb\sqrt{\rho} \quad (4)$$

where $M = m^{-1}$ is the Taylor factor of pure Mg and m is the Schmid factor, α is a dimensionless constant, and G is the shear modulus of pure Mg.

The yield strengths of the samples were calculated for different deformation conditions and the results are shown in Table 3. It is readily apparent that the calculated yield strengths are in reasonable agreement with the measured experimental values and this supports the validity of these calculations. Based on the calculations in Table 3, the percentage contributions of grain

Table 3. Contributions of different strengthening mechanisms to the yield strength of pure Mg (MPa).

Turns	293 K			423 K		
	1/8	1	10	1/8	1	10
Measured yield strength	112 ± 3	132 ± 4	148 ± 5	118 ± 3	112 ± 3	113 ± 3
σ_0	31	31	31	31	31	31
σ_{gb}	35 ± 2	56 ± 1	78 ± 1	59 ± 1	75 ± 1	78 ± 1
σ_{dis}	41 ± 2	46 ± 2	51 ± 1	36 ± 2	17 ± 2	17 ± 2
$\sigma_{0.2} = \sigma_0 + \sigma_{\text{gb}} + \sigma_{\text{dis}}$	107 ± 4	133 ± 3	160 ± 2	126 ± 4	123 ± 3	126 ± 2

Table 4. Percentage contributions of different strengthening mechanisms to the yield strength of pure Mg based on the calculations in Table 3.

Turns	293 K			423 K		
	1/8	1	10	1/8	1	10
σ_0	29%	23%	19%	25%	25%	25%
σ_{gb}	33%	42%	46%	47%	61%	62%
σ_{dis}	38%	35%	32%	29%	14%	13%
$\sigma_{0.2} = \sigma_0 + \sigma_{\text{gb}} + \sigma_{\text{dis}}$	100%	100%	100%	100%	100%	100%

size and dislocation density to the yield strength of materials processed by HPT at 293 and 423 K are summarized in Table 4. The dislocation-induced strengthening in samples processed by HPT at 473 K gradually decreases from 29% for the 1/8 turn sample to 13% for the ten turns sample. The dislocation-induced strengthening in samples processed by HPT at 293 K slightly decreases from 38% for the 1/8 turn sample to 32% for the ten turns sample, and this confirms that some recovery and recrystallization occurred during room temperature processing.

5. Summary and Conclusions

Pure Mg with an initial grain size of $\approx 45 \mu\text{m}$ was processed by high-pressure torsion up to 10 turns at temperatures of 293 and 423 K. Fine-grained microstructures were obtained after ten turns of HPT processing with bimodal grain sizes and minimum grain sizes of $\approx 2 \mu\text{m}$ at both 293 and 423 K.

The grain refinement processes were different at these different processing temperatures. At 293 K the microstructure was gradually refined with an accumulation of strain and dynamic recrystallization occurred when the rotation reached ≈ 10 turns. At 423 K grain refinement occurred by dynamic recrystallization at all HPT processing strains.

Grain boundary strengthening is the most important factor affecting the yield strength of pure Mg. When the dislocation density reaches 10^{15}m^{-2} at 293 K, dislocation strengthening also made an important contribution to the yield strength. The samples processed by HPT at 293 K exhibited low uniform elongations.

Significant bimodal grain structures were formed in pure Mg after multiple turns of HPT processing at 423 K and the dislocation densities were then relatively low due to the dynamic recrystallization process.

Acknowledgements

The work of two of the authors (Y.H. and T.G.L.) was supported by the European Research Council under ERC Grant Agreement No. 267464-SPDMETALS.

Conflict of Interest

The authors declare no conflict of interest.

Data Availability Statement

The data that support the findings of this study are available from the corresponding author upon reasonable request.

Keywords

bimodal structures, high-pressure torsion, magnesium, microstructure evolution, strengthening mechanisms

Received: June 4, 2022

Revised: June 26, 2022

Published online: July 17, 2022

- [1] B. L. Mordike, T. Ebert, *Mater. Sci. Eng., A* **2001**, 302, 37.
- [2] M. M. Avedesian, *Magnesium and Magnesium Alloys* (Ed: H. Baker), ASM International, Materials Park, OH, USA **1999**.
- [3] E. O. Hall, *Proc. Phys. Soc. Lond. B* **1951**, 64, 747.
- [4] N. J. Petch, *J. Iron and Steel Inst.* **1953**, 174, 25.
- [5] R. Armstrong, R. M. Douthwaite, I. Codd, N. J. Petch, *Phil. Mag.* **1962**, 7, 45.
- [6] M. Mabuchi, K. Higashi, *Acta Mater.* **1996**, 44, 4611.
- [7] N. Balasubramanian, T. G. Langdon, *Metall. Mater. Trans. A* **2016**, 47A, 5827.
- [8] R. B. Figueiredo, T. G. Langdon, *J. Mater. Res. Tech.* **2021**, 14, 137.
- [9] R. Z. Valiev, R. K. Islamgaliev, I. V. Alexandrov, *Prog. Mater. Sci.* **2000**, 45, 103.
- [10] R. Z. Valiev, Y. Estrin, Z. Horita, T. G. Langdon, M. J. Zehetbauer, Y. T. Zhu, *JOM* **2006**, 58, 33.
- [11] C. P. Wang, F. G. Li, B. Chen, Z. W. Yuan, H. Y. Lu, *Rare Met. Mater. Eng.* **2012**, 41, 941.
- [12] R. Z. Valiev, Y. Estrin, Z. Horita, T. G. Langdon, M. J. Zehetbauer, Y. T. Zhu, *JOM* **2016**, 68, 1216.
- [13] R. Z. Valiev, Y. Estrin, Z. Horita, T. G. Langdon, M. J. Zehetbauer, Y. T. Zhu, *Mater. Res. Lett.* **2016**, 4, 1.
- [14] R. Z. Valiev, B. Straumal, T. G. Langdon, *Ann. Rev. Mater. Res.* **2022**, 52, 357.
- [15] R. Z. Valiev, T. G. Langdon, *Prog. Mater. Sci.* **2006**, 51, 881.
- [16] A. P. Zhilyaev, T. G. Langdon, *Prog. Mater. Sci.* **2008**, 53, 893.
- [17] R. B. Figueiredo, P. R. Cetlin, T. G. Langdon, *Acta Mater.* **2007**, 55, 4769.
- [18] F. Kang, J. T. Wang, Y. Peng, *Mater. Sci. Eng., A* **2008**, 487, 68.
- [19] Y. Huang, R. B. Figueiredo, T. Baudin, F. Brisset, T. G. Langdon, *Adv. Eng. Mater.* **2012**, 14, 1018.
- [20] Y. Huang, R. B. Figueiredo, T. Baudin, A.-L. Helbert, F. Brisset, T. G. Langdon, *Mater. Res.* **2013**, 16, 577.
- [21] A. P. Zhilyaev, B. K. Kim, K. V. Nurislamova, M. D. Baró, J. A. Szpunar, T. G. Langdon, *Scr. Mater.* **2002**, 46, 575.
- [22] A. P. Zhilyaev, G. V. Nurislamova, B. K. Kim, M. D. Baró, J. A. Szpunar, T. G. Langdon, *Acta Mater.* **2003**, 51, 753.
- [23] J. Wongsan-Ngam, M. Kawasaki, T. G. Langdon, *J. Mater. Sci.* **2013**, 48, 4653.
- [24] J. Čížek, I. Procházka, B. Smola, I. Stulíková, R. Kužel, Z. Matěj, V. Cherkaska, R. K. Islamgaliev, O. Kulyasova, *Mater. Sci. Eng., A* **2007**, 462, 121.
- [25] B. J. Bonarski, E. Schafner, B. Mingler, W. Skrotzki, B. Mikulowski, M. J. Zehetbauer, *J. Mater. Sci.* **2008**, 43, 7513.
- [26] M. Kai, Z. Horita, T. G. Langdon, *Mater. Sci. Eng., A* **2008**, 488, 117.
- [27] D. Arpacay, S. Yi, M. Janeček, A. Bakkaloglu, L. Wagner, *Mater. Sci. Forum* **2008**, 584, 300.
- [28] Y. Harai, M. Kai, K. Kaneko, Z. Horita, T. G. Langdon, *Mater. Trans.* **2008**, 49, 76.
- [29] B. J. Bonarski, E. Schafner, B. Mikulowski, M. J. Zehetbauer, *J. Phys.: Conf. Series* **2010**, 240, 012133.
- [30] P. Serre, R. B. Figueiredo, N. Gao, T. G. Langdon, *Mater. Sci. Eng., A* **2011**, 528, 3601.
- [31] K. Edalati, A. Yamamoto, Z. Horita, T. Ishihara, *Scr. Mater.* **2011**, 64, 880.
- [32] Y. Huang, R. B. Figueiredo, T. G. Langdon, *Rev. Adv. Mater. Sci.* **2012**, 31, 129.
- [33] S. A. Torbati-Sarraf, T. G. Langdon, *J. Alloys Compd.* **2014**, 613, 357.
- [34] F. Q. Meng, J. M. Rosalie, A. Singh, J. Somekawa, K. Tsuchiya, *Scr. Mater.* **2014**, 78, 57.
- [35] X. G. Qiao, Y. W. Zhao, W. M. Gan, Y. Chen, M. Y. Zheng, K. Wu, N. Gao, M. J. Starink, *Mater. Sci. Eng., A* **2014**, 619, 95.
- [36] M. Joshi, Y. Fukuta, S. Gao, N. Park, D. Terada, N. Tsuji, *IOP Conf. Series: Mater. Sci. Eng.* **2014**, 63, 012074.
- [37] J. Stráská, M. Janeček, J. Gubicza, T. Krajňák, E. Y. Yoon, H. S. Kim, *Mater. Sci. Eng., A* **2015**, 625, 98.
- [38] O. B. Kulyasova, R. K. Islamgaliev, Y. H. Zhao, R. Z. Valiev, *Adv. Eng. Mater.* **2015**, 17, 1738.
- [39] S. V. Dobatkin, L. L. Rokhlin, E. A. Lukyanova, M. Yu. Murashkin, T. V. Dobatkina, N. Yu. Tabachkova, *Mater. Sci. Eng., A* **2016**, 667, 217.
- [40] R. Alizadeh, R. Mahmudi, A. H. W. Ngan, Y. Huang, T. G. Langdon, *Mater. Sci. Eng., A* **2016**, 651, 786.
- [41] C. Z. Zhang, S. J. Zhu, L. G. Wang, R. M. Guo, G. C. Yue, S. K. Guan, *Mater. Des.* **2016**, 96, 54.
- [42] R. B. Figueiredo, F. S. J. Poggiali, C. L. P. Silva, P. R. Cetlin, T. G. Langdon, *J. Mater. Sci.* **2016**, 51, 3013.
- [43] R. B. Figueiredo, S. Sabbaghianrad, A. Giwa, J. R. Greer, T. G. Langdon, *Acta Mater.* **2017**, 122, 322.
- [44] R. B. Figueiredo, S. Sabbaghianrad, T. G. Langdon, *IOP Conf. Ser. Mater. Sci. Eng.* **2017**, 194, 012039.
- [45] W. T. Sun, C. Xu, X. G. Qiao, M. Y. Zheng, S. Kamado, N. Gao, M. J. Starink, *Mater. Sci. Eng., A* **2017**, 700, 312.
- [46] Y. I. Bourezg, H. Azzeddine, T. Baudin, A.-L. Helbert, Y. Huang, D. Bradai, T. G. Langdon, *Mater. Sci. Eng., A* **2018**, 724, 477.
- [47] K. Bryla, J. Morgiel, M. Faryna, K. Edalati, Z. Horita, *Mater. Lett.* **2018**, 212, 323.
- [48] S. A. Torbati-Sarraf, S. Sabbaghianrad, T. G. Langdon, *Adv. Eng. Mater.* **2018**, 20, 1700703.
- [49] D. Ahmadvani, Y. Huang, M. Jaskari, A. Jarvenpaa, M. H. Sohi, C. Zanella, L. P. Karjalainen, T. G. Langdon, *J. Mater. Sci.* **2018**, 53, 16585.
- [50] A. Hanna, H. Azzeddine, R. Lachhab, T. Baudin, A.-L. Helbert, F. Brisset, Y. Huang, D. Bradai, T. G. Langdon, *J. Alloys Compd.* **2019**, 778, 61.
- [51] W. Li, X. Liu, Y. Zheng, W. Wang, W. Qiao, K. W. Yeung, K. M. C. Cheung, S. Guan, O. B. Kulyasova, R. Z. Valiev, *Biomater. Sci.* **2020**, 8, 5071.
- [52] R. B. Figueiredo, P. H. R. Pereira, T. G. Langdon, *Adv. Eng. Mater.* **2020**, 22, 1900565.
- [53] Y. I. Bourezg, H. Azzeddine, K. Abib, Y. Huang, D. Bradai, T. G. Langdon, *J. Mater. Res. Technol.* **2020**, 9, 3047.
- [54] R. B. Figueiredo, T. G. Langdon, *Metals* **2020**, 10, 681.
- [55] Y. I. Bourezg, H. Azzeddine, M. Harfouche, D. Thiaudiere, C. Mocuta, Y. Huang, D. Bradai, T. G. Langdon, *Mater. Lett.* **2020**, 264, 127379.
- [56] H. Somekawa, J. Yi, A. Singh, K. Tsuchiya, *Mater. Sci. Eng., A* **2021**, 823, 141735.

- [57] N. X. Zhang, M. Kawasaki, Y. Huang, T. G. Langdon, *Mater. Sci. Eng., A* **2021**, *906*, 140832.
- [58] R. B. Figueiredo, T. G. Langdon, *Adv. Eng. Mater.* **2019**, *21*, 1801039.
- [59] R. B. Figueiredo, P. R. Cetlin, T. G. Langdon, *Mater. Sci. Eng., A* **2011**, *528*, 8198.
- [60] R. B. Figueiredo, P. H. R. Pereira, M. T. P. Aguilar, P. R. Cetlin, T. G. Langdon, *Acta Mater.* **2012**, *60*, 3190.
- [61] D. A. Hughes, N. Hansen, *Acta Mater.* **1997**, *45*, 3871.
- [62] T. G. Langdon, *Mater. Sci. Eng., A* **2007**, *462*, 3.
- [63] H. Azzeddine, D. Bradai, T. Baudin, T. G. Langdon, *Prog. Mater. Sci.* **2022**, *125*, 100886.
- [64] I. Dragomir, T. Ungár, *J. Appl. Crystallog.* **2002**, *35*, 556.
- [65] K. Máthis, K. Nyilas, A. Axt, I. Dragomir-Cernatescu, T. Ungár, P. Lukáč, *Acta Mater.* **2004**, *52*, 2889.
- [66] Y. Estrin, A. Molotnikov, C. H. J. Davies, R. Lapovok, *J. Mech. Phys. Solids* **2008**, *56*, 1186.
- [67] E. W. Hart, *Acta Metall.* **1967**, *15*, 351.
- [68] X. X. Huang, N. Hansen, N. Tsuji, *Science* **2006**, *312*, 249.
- [69] H. Zhang, H. Y. Wang, J. G. Wang, J. Rong, M. Zha, C. Wang, P. K. Ma, Q. C. Jiang, *J. Alloys Compd.* **2019**, *780*, 312.
- [70] M. Zha, H. M. Zhang, Z. Y. Yu, X. H. Zhang, X. T. Meng, H. Y. Wang, Q. C. Jiang, *J. Mater. Sci. Technol.* **2018**, *34*, 257.
- [71] Z. Z. Jin, M. Zha, Z. Y. Yu, P. K. Ma, Y. K. Li, J. M. Liu, H. L. Jia, H. Y. Wang, *J. Alloys Compd.* **2020**, *833*, 155004.
- [72] Y. D. Qiao, X. Wang, Z. Y. Liu, E. D. Wang, *Mater. Sci. Eng., A* **2013**, *578*, 240.
- [73] S. M. Yin, C. H. Wang, Y. D. Diao, S. D. Wu, S. X. Li, *J. Mater. Sci. Technol.* **2011**, *27*, 29.
- [74] A. Sanaty-Zadeh, *Mater. Sci. Eng., A* **2012**, *531*, 112.